Chapter 7
Circularly Polarized High Harmonic Generation for Probing Molecular Chirality

Taro Sekikawa, Kengo Ito, Eisuke Haraguchi, and Keisuke Kaneshima

Abstract Chirality of molecules play an important role in biological activity. Chiral molecules are not superimposable on their own mirror images, called enantiomers, and do not have a symmetry plane nor a center of inversion symmetry. The chemical reactivity of the enantiomers sometimes depends on the chirality. Hence the distinguishing the enantiomers is important and circularly polarized light has been used to discern the enantiomers for a long time. The development of ultrashort pulse technology enables us to investigate nonlinear interactions of chiral molecules with an intense light field. Among various nonlinear optical interactions, we focus on high harmonic generation as the probe into molecular chirality. Here, we describe two our recent results: one is circularly polarized high harmonic generation (CP-HHG) from a chiral molecule, limonene, driven by a CP counter-rotating two-color laser field. The other is the development of elliptically polarized single-order high harmonic light source for the application to photoelectron spectroscopy of chiral molecules.

The physical properties of the enantiomers of chiral molecules are same. However, the chemical reactivity exhibits a strong enantiomeric selectivity. Therefore, the chirality plays a decisive role in biological systems. Discerning the enantiomers is important for understanding the activities of chiral molecules in biological systems. It is interesting that the interaction between circularly polarized (CP) light and chiral molecules depend on the chirality. Therefore, CP light has been used to investigate the magnetic properties and chirality of materials. The development of high peak power lasers provides us new opportunities to explore nonperturbative nonlinear interactions of chiral molecules with an optical field.

Among many nonlinear optical interactions, we are interested in high harmonic generation (HHG) as a probe into molecular chirality. Recently, using the approach based on HHG, the observation of molecular chirality was reported [1–3]. HHG is the light field emission by the nonlinear interactions between a laser electric field and the interacting molecules [4]. The process of HHG is intuitively understood by

T. Sekikawa (✉) · K. Ito · E. Haraguchi · K. Kaneshima
Department of Applied Physics, Hokkaido University, Sapporo 060-8628, Japan
e-mail: sekikawa@eng.hokudai.ac.jp

K. Yamanouchi et al. (eds.), *Progress in Ultrafast Intense Laser Science XVI*,
Topics in Applied Physics 141, https://doi.org/10.1007/978-3-030-75089-3_7

the three-step model, where an electron (1) is ionized by tunneling from an atom or molecule in the presence of a strong laser field, (2) is accelerated in the laser field, and (3) recombines with the parent ion and then emits a higher harmonic photon with an energy corresponding to the sum of the kinetic and ionization energies [5]. Because the HHG yield depends on the electronic states of the interacting molecules through tunneling and recombination probabilities, HHG can be used to probe the electronic states of the molecules, including the symmetry or the chirality of the molecular orbitals. This spectroscopic approach is known as high harmonic spectroscopy (HHS).

HHG can also be used as a light source to probe the chirality. Extreme ultraviolet (EUV) light, which has a high photon energy, allows element selective probing. Accordingly, CP EUV light enables the investigation of element selective electromagnetic and chiral phenomena [6]. High harmonics (HHs) of ultrashort laser pulses [7, 8] are promising for such investigations owing to their spatial and temporal coherence transferred from the driving laser. The electromagnetic fields of HHs are well polarized, and the temporal width of the HH pulses breaks into the attosecond regime [9–13].

In this article, we describe our recent investigation on the circular dichroism (CD) in HHG from chiral molecules [14] and on the polarimetry of elliptically polarized HHG [15]. The former is a kind of HHS to gain insight into chirality. The latter is for the development of a single-order CP EUV light source for the observation of the CD of chiral molecules.

7.1 Circular Dichroism in High Harmonic Generation from Chiral Molecules

7.1.1 Introduction

To distinguish between the enantiomers in a condensed phase, optical approaches such as the CD of photoabsorption and the optical rotation of light polarization have been used. These effects are induced by the interference term $\vec{\mu} \cdot \vec{m}$ between the electric $\vec{\mu}$ and magnetic $\vec{m}$ dipoles in the transition moment [16]. As $\left|\vec{m}\right|$ is generally small, the magnitude of the CD of photoabsorption is typically on the order of 10^{-4}–10^{-5}. Therefore, discerning the enantiomers is a demanding task. However, in the gas phase, the spatial distribution of the photoelectron emission from chiral molecules was found to have a larger anisotropy than the CD of photoabsorption by two or three orders of magnitude, enabling the observation or determination of the molecular chirality with a higher sensitivity [17–20].

HHG provides us unique opportunities for the investigation of chirality. In [1], HHS was applied to detect the chirality based on the observation that the HHG yield from chiral molecules is asymmetric with respect to the sign of the degree of the ellipticity of the driving laser. The ellipticity maximizing the anisotropy was found

to be ±1–2%. This anisotropy comes from the transition between electronic states in the cation, dependent on $\overrightarrow{m}$ pertinent to the molecule, during the second step of the three-step model. The recombining state of the cation with the free electron during the third step could be different from the initial state upon tunneling ionization, resulting in a difference in HHG yield. The interstate transition during the second step is sensitive to the sign of $\overrightarrow{m}$. Thus, the HHG yield is chiral-sensitive.

Previously, we investigated the CD of the CP-HHG by a two-color bicircular laser field from chiral molecules [14]. We used a photoelectron spectrometer using Kr gas as a target. However, the sensitivity to HHG was low. Therefore, in this study, we employed an EUV spectrometer equipped with a charge-coupled device (CCD) camera and observed the CD with better sensitivity to HHG.

CP HHG from a single-color CP laser beam is prohibited by the conservation of spin angular momentum. Considering the three-step model, the released electron cannot return to the parent ion under a CP light field, resulting in no HHG. Therefore, in [1], the polarization of the used laser pulses was very close to linear, as described above. In contrast, a two-color CP laser fields with counter-rotating polarizations generate CP high harmonic pulses [21–30]. The synthesized laser field by the fundamental (ω) and its second-harmonic (2ω) CP light exhibits a three-fold spatiotemporal symmetry. Therefore, the $3m$-order harmonics are missing in isotropic media, where m is a positive integer [23, 25]. The circular polarizations of the $3m + 1$ and $3m + 2$ harmonics are the same as those of ω and 2ω, respectively, and are opposite to each other because of the conservation of spin angular momentum. In this study, we observed the CD of CP HHG from the enantiomers of 1-methyl-4-(prop-1-en-2-yl)cyclohex-1-ene (limonene, inset of Fig. 7.1).

These enantiomers act differently in our smell of sense, e.g., each enantiomer has a peculiar smell: (*R*)- and (*S*)-limonene have the fragrance of oranges and pine, respectively. When light with a linear polarization passes through a pure enantiomer, the plane of polarization is rotated [31]. This is known as optical rotation. (*R*)- and (*S*)-limonene molecules rotate the plane clockwise or counterclockwise as viewed by an observer facing the oncoming wave, respectively.

In the quantum mechanical expression of the three-step model of HHG, the third step is expressed as the complex conjugate of the transition dipole moment between the ground state and ionized state [21, 24, 27, 32, 33]. Therefore, the CP HHG yield is expected to depend on the symmetry of the wavefunction of the outermost atomic or molecular orbital [9, 12]. Experimentally, the relative intensities of the allowed neighboring harmonics, $3m + 1$ and $3m + 2$, in CP HHG were found to depend on the atomic species [27, 29]. In the early stage of the investigation, these relative intensities appeared to be understood by the following propensity rule: single photoionization with a field corotating with the initial state is much more likely than with a counter-rotating field [24, 27]. However, the underlying mechanism was found to be more complicated, and precise theoretical calculations are necessary to understand it completely [29].

Although the quantitative prediction of the relative intensities is not simple, the sensitivity of CP HHG to the outermost atomic orbital suggests that CP HHG is also susceptible to the highest occupied molecular orbital (HOMO) of a chiral molecule,

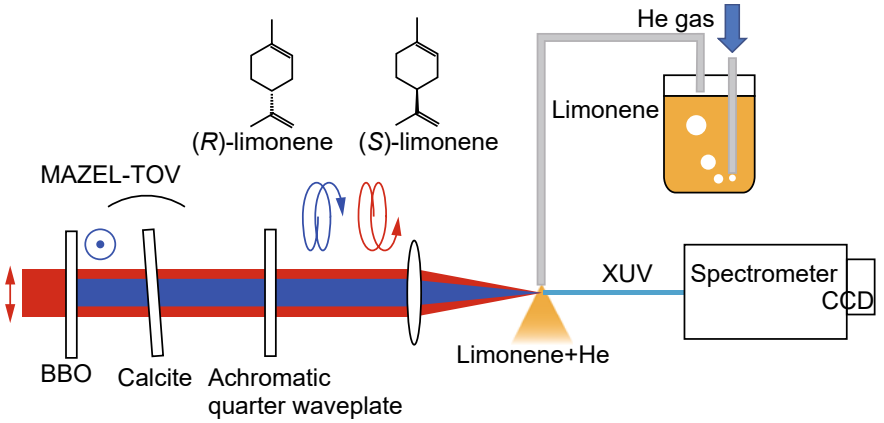

Fig. 7.1 Experimental setup for the observation of CP HHG. MAZEL-TOV is the optical system used to generate the two-color counter-rotating CP laser field consisting of a BBO crystal, a calcite plate, and an AQW [34]. The superposition of the two-color counter-rotating polarized laser fields, of which the rotation directions of the fundamental and second-harmonic light field are represented by the counterclockwise and clockwise arrows, respectively, forms triangular polarization with threefold symmetry. The inset is the molecular structures of limonene molecules

the direction of which should be determined by the rotation direction of the electrons in the HOMO. Even for randomly oriented molecules, the chirality is active. This indicates that CP HHG can be used to discern molecular chirality. Still, the response of a large molecule to a laser field would not be as simple as that of an atomic orbital. Therefore, the purpose of the present work is the experimental exploration of the sensitivity of CP HHG to molecular chirality.

7.1.2 Experiment

The experimental setup for CP HHG is illustrated in Fig. 7.1. A Ti:sapphire laser system delivers 1.4 mJ, 35 fs pulses with a center wavelength of 800 nm at a repetition rate of 1 kHz. The two-color counter-rotating CP laser field was synthesized by the inline setup called MAZEL-TOV [34]: the linearly polarized 800 nm pulses were partially converted to 400-nm pulses with a polarization perpendicular to ω by a β-BaB_2O_4 (BBO) crystal with a thickness of 300 μm. The pulse energies of the ω and 2ω pulses were 0.9 and 0.5 mJ, respectively. After compensating the group-delay between the ω and 2ω pulses by a calcite plate, their polarizations were changed to circular by an achromatic quarter-waveplate (AQW) (Kogakugiken corp.). Here, the rotation directions of the ω and 2ω were opposite to each other and were switched just by rotating the crystal axis of the AQW by 90°. Because of the inline setup, the spatial overlap between the ω and 2ω beams was suitable to form a triangular electric field. The generation of the $3m$-th harmonics was almost suppressed. In this paper,

counterclockwise polarization is defined by an observer facing an oncoming wave and vice versa.

The two-color synthesized laser field was focused into a gas jet using a concave mirror with a focal length of 0.5 m. The gas jet was formed by a glass capillary with an inner diameter of 300 μm. The capillary tip was set at the focal point of the mirror. The peak intensities of the ω and 2ω beams were estimated to be 5.0×10^{14} and 1.4×10^{14} W/cm^2, respectively. The enantiomers of limonene molecules, purchased from Wako Pure Chemical Industries Ltd., were stored in a glass bubbler and warmed to 333 K to increase their vapor pressure. The limonene vapor was sent through a heated pipeline to the glass capillary mixed with 1.6 atm helium gas. The flow of the limonene molecules mixed with helium was continuous. The spectra of the high harmonics were recorded by an EUV spectrometer with a CCD camera. The intensity of each harmonic was obtained by integrating the counts of each peak, and the ambiguity of the intensity was estimated by the square root of the total counts.

7.1.3 Results and Discussion

Figure 7.2a and b present the spectra of the CP HHG from (*S*)-limonene, and (*R*)-limonene, respectively. The clockwise (counterclockwise) circular arrow in Fig. 7.2 indicates the rotation direction of the polarization of the ω (2ω) used for HHG. The dotted (solid) lines indicate the CP HHG spectra generated by the combination of a clockwise (counterclockwise) rotating ω and counterclockwise (clockwise) rotating 2ω represented by the solid and dotted arrows, respectively. The following two features in the spectra are identified: (1) The $3m + 1$ harmonics of the (*R*)-limonene signal are relatively more enhanced than the $3m + 2$ when the ω has a clockwise polarization. (2) However, for the counterclockwise polarization of the ω, the $3m + 1$ harmonics of the (*S*)-limonene signal are more enhanced.

To quantitatively evaluate the CD, the Kuhn g-factor 2(IL - IR)/(IL + IR), where IL and IR are the intensities with counterclockwise and clockwise polarization, respectively, was estimated by summing up the counts for each harmonic order after normalizing the total counts of the observed spectrum to the same value for each polarization and is shown in Fig. 7.3. (*R*)-limonene (triangle) generates more high harmonics with clockwise circular polarization than with counterclockwise circular polarization, while (*S*)-limonene (circle) prefers the generation of harmonics with counterclockwise circular polarization. The Kuhn g-factors are almost symmetrical with respect to the baseline, indicating the CD in HHG. These results are consistent with the previous results [14].

Under the present experimental conditions, the interaction length between the laser field and chiral molecules was 300 μm and the gas density of the chiral molecules was low. Therefore, the phase-mismatch among the driving laser pulses and high harmonic pulses was negligible [25, 27, 35], which will be evaluated later. The response of a single molecule should be crucial for dichroism. The observed CD would be explained by the same processes proposed in [1] and [33]: the transition

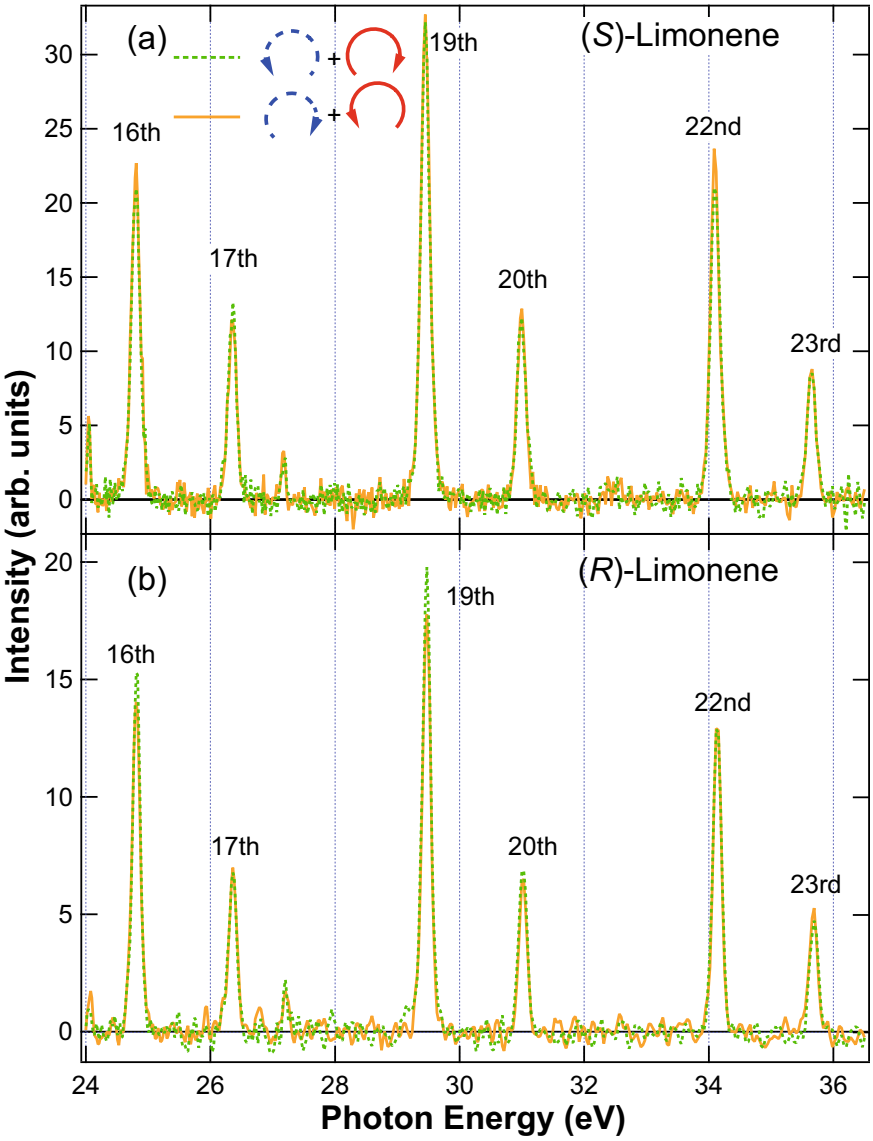

Fig. 7.2 High harmonics spectra from **a** He, **b** (*S*)-limonene, and **c** (*R*)-limonene, generated by the synthesized laser field by the CP ω and 2ω. The spectra shown by the dotted (solid) lines have been generated by the combination of ω and 2ω, of which the rotational directions of the polarization are clockwise (counterclockwise), represented by solid arrow, and counterclockwise (clockwise), represented by dotted arrow, respectively

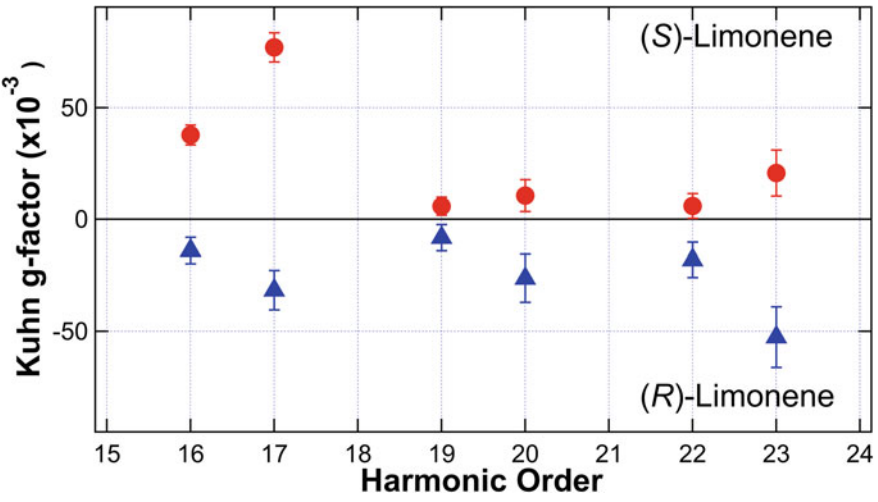

Fig. 7.3 Kuhn g-factors from the enantiomers for each higher harmonic order

to another state by $\overrightarrow{m}$ in the cation during the second step of the three-step model modulates the efficiency of HHG.

Here, however, more intuitive perspectives may be provided. One is the propensity rule of the ionization probability dictating the third process of the three-step model [24, 27, 29]: the emitted radiation is more likely to acquire a polarization with the same rotation direction of the outermost atomic orbitals [24]. Therefore, the preferred CP HHG is determined by the rotation direction of the HOMO wavefunction of an enantiomer, although it is not straightforward to predict the direction of the rotation or the ring current in the molecule from the molecular structure or the distribution of the HOMO electrons. Further investigation on HHG from chiral molecules will reveal the relationship between them.

As another perspective, the resonance with the intermediate states with CD could be responsible for the CD in HHG. In perturbative nonlinear optics, it is well-known that the resonance with the electronic states of nonlinear media enhances the nonlinear susceptibility. Even in HHG, the resonance with an electronic state raises the generation efficiency [36]. The photoabsorption of limonene appears in a wavelength region shorter than about 220 nm with CD [37]. Thus, both ω and 2ω can be resonant with the states at 200 nm. Because (*R*)-limonene has a larger absorption coefficient for clockwise polarization at 200 nm [37], the nonlinear responses to the clockwise polarized light could be larger at 200 nm than to the counterclockwise polarization. Experimentally, the Kuhn g-factors are found to have a negative sign for (*R*)-limonene, as shown in Fig. 7.3. That is, the HHs with clockwise polarization were generated more efficiently from (*R*)-limonene. Considering that the $3m + 1$ and $3m + 2$ orders have the same polarization as ω and 2ω, respectively [25], the resonance of ω or 2ω, with clockwise polarization, with the dichroic states enhances the HHs with clockwise polarization from (*R*)-limonene.

CD of the states at about 200 nm in limonene was observed in the photoelectron spatial distribution: Fanood et al. observed the wavelength dependence of the anisotropy of the photoelectron emission by the (2+1) resonance multiphoton ionization by the CP photons [38]. They found that the sign of the asymmetry factor of the photoemission from the HOMO was reversed when the center wavelength of the laser was changed from 420 to 392 nm. Interestingly, at these wavelengths, the sign of the CD of linear absorption also reversed [37]. This correspondence between the CD of the photoelectron emission and that of the linear absorption is attributed to the resonance with different vibrational levels and different electronic ion core configurations in the intermediate Rydberg states [38]. The intermediate states with CD should also influence the HHG through the resonance effects.

The enhancement of CP HHG by the resonance with the intermediate states with CD also appears to be the case in [1]. It was found that an elliptically polarized driving laser rotating in the clockwise direction with photon energies of 0.70 and 0.67 eV generates high harmonics more efficiently from (*S*)-epoxypropane and (*R*)-fenchone than the laser field rotating in the opposite direction. According to [39, 40], (*S*)-epoxypropane and (*R*)-fenchone are resonant and have larger absorption coefficients at 11 (=7.7 eV) and 6 photons (=4.0 eV) for the clockwise polarization, respectively. The correspondence found in limonene predicts that HHs are generated more efficiently by the driving laser with the clockwise polarization from these enantiomers, and successfully explains the experimental observation.

Finally, the phase mismatch in CP-HHG was estimated as follows. The angle of the optical rotation α and the difference in the refractive indices of the circular polarizations Δn have the relation of $\alpha = \pi \Delta n l/\lambda$, where λ and l are the wavelength and interaction length, respectively. Using α and n given in [31], Δn at ω and 2ω was deduced to be 2.1×10^{-6} and 5.2×10^{-6}, respectively, for a 1 cm-long liquid. As Δn is proportional to the density of limonene, Δn in the gas phase was estimated considering the vapor pressure [41]; at 358 K, the vapor pressure was 4.92 kPa. If the total gas pressure just below the capillary tube was 2700 Pa [42], the pressure of limonene was estimated as 82 Pa. When the temperature was cooled to 100 K by supersonic expansion, the gas density of limonene was 1.4×10^{-5} g/cm^3. As Δn is proportional to the density and the interaction length l of 300 μm, Δn at 2ω and ω are 8.2×10^{-11} and 3.3×10^{-11}, respectively. Meanwhile, the corresponding average refractive indices are 1.00026 and 1.00025, respectively. Therefore, under the assumption that the refractive indices in the EUV range are unity, the difference in the phase mismatch coming from the CD is negligibly small and phase matching is not the primary effect.

In summary, the CP HHG limonene enantiomer spectra were found to exhibit CD in the intensities. CP HHG is sensitive to the chirality of the interacting molecules with a synthesized CP light field. CP HHG appears to be very promising for discriminating enantiomers. As CP HHG includes processes taking place on the attosecond timescale, CP HHG might also be applicable to probe the attosecond transient chirality of molecules.

7.2 Polarimetry of a Single-Order Circularly Polarized High Harmonic Separated by a Time-Delay Compensated Monochromator

7.2.1 Introduction

To generate CP EUV light, the polarization conversion from linear to circular polarization was demonstrated by a reflective polarizer, although the conversion efficiency was ~4% [6]. Recently, the generation scheme of CP HHs directly driven by laser field was established [23, 25, 34, 43–45]. The driving laser field synthesized by two-color CP light fields with counter-rotating circular polarizations enables the efficient generation of CP HHs, while the one-color single beam CP laser field does not generate HHs, underlain by the three-step model of HH generation [5] and by the conservation of the spin angular momentum of photons. The conversion efficiency is comparable to the linearly polarized HH generation [23]. In the case of noncollinear geometry [43, 44], the HHs generated by two noncolinear beams with the same color are spatially dispersed. The propagating direction of each HH is determined by the conservation of the spin angular momentum of photons.

The application of CP HHs sometimes requires focusing the single-order harmonic on a target. However, in collinear geometry, all harmonics spatially overlap. Thus, it is necessary to spatially separate the harmonics. Although the harmonic orders are spatially dispersed in noncollinear geometry [43], it is not tractable to focus a specific harmonic order on targets. The usage of a grating is more convenient to both separate and focus the beam, as has already been demonstrated in the observation of nanoscale magnetic imaging [46].

Here, the monochromatization and focusing of a CP harmonic generated in the collinear scheme was implemented by a time-delay compensated monochromator (TDCM) [47–49], consisting of a pair of toroidal gratings and a slit [15]. The TDCM preserves the pulse duration of the selected harmonic [47–49] and focuses the harmonic pulses on target [48]. The TDCM is extensively used for time-resolved photoelectron spectroscopy using a linearly polarized harmonic [50–52]. To assess the applicability of the TDCM to isolate a single-order CP harmonic, the ellipticity of the selected harmonic was evaluated, because the grazing incidence to the toroidal gratings in the TDCM distorts the circular polarization to elliptical owing to the anisotropy of the complex coefficient of the diffraction on the grating. To obtain a CP HH, elliptically polarized harmonic pulses were generated by manipulating the polarization of the driving laser field and were corrected by the diffraction by the gratings. The first practical isolation and characterization of a CP single-order harmonic is demonstrated.

7.2.2 Experiment

The experimental setup is shown in Fig. 7.4. The driving laser field was synthesized by the MAZEL-TOV scheme described in Sect. 7.1.2 [34]. The 900 μJ, 35 fs linearly polarized ω light delivered at 1 kHz by a Ti:sapphire laser system was partially converted to 300 μJ 2ω light with perpendicular polarization to ω by a BBO crystal. The circular polarizations of HHs were switched by rotating the AQW by 90°. The ellipticity of ω and 2ω were 0.99 and 0.98, respectively, measured using a linear polarizer and a quarter waveplate. In this section, the rotating direction of the circular polarization is also defined as viewed by an observer facing the oncoming light, which is same in the previous section. The counterclockwise and clockwise rotations of the light polarization are called left-handed (LH) and right-handed (RH) polarization, respectively. Because MAZEL-TOV is composed of static optical elements, the relative phase between ω and 2ω was fixed. The two CP beams were focused in a Kr gas jet by a concave mirror with a 50 cm focal length. The inset in Fig. 7.4 shows the photoelectron spectrum of Kr atoms irradiated by HHs. Each labeled harmonic order has two peaks because of the spin–orbit splitting of the cation. The generation of the 18th harmonic was suppressed, and its intensity was 18% and 0.7% of the 19th and 17th harmonics, respectively, reinforcing the three-fold symmetry of the synthesized driving laser field. Therefore, the generated HHs were expected to be highly CP. The TDCM consists of a pair of Pt-coated toroidal gratings (HORIBA JOBIN YVON, 54,000,910) and the slit [48, 49]. The first grating disperses the harmonics spatially, and the slit selects a single-order harmonic. The second grating compensates for the pulse front tilt introduced by the diffraction to compress the pulse duration. The reflection angle of the grating is 142°. The harmonic order

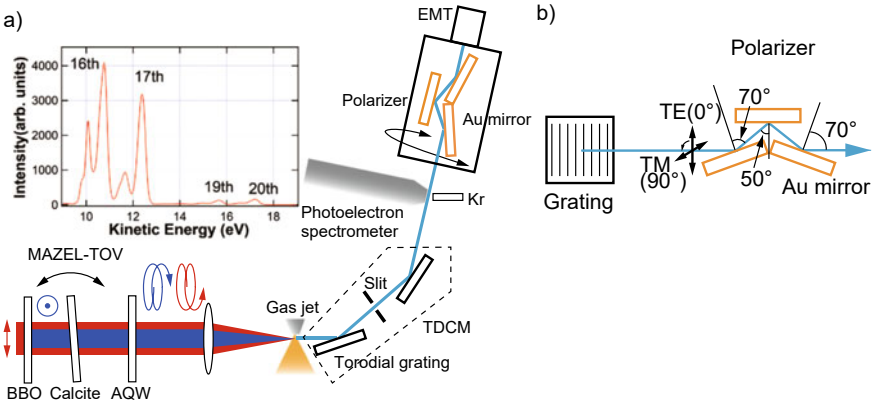

Fig. 7.4 **a** Experimental setup. AQW is an achromatic quarter waveplate, and EMT is an electron multiplier. TDCM is a time-delay compensated monochromator. The inset shows the photoelectron spectrum of Kr atoms irradiated by the labeled high harmonics. **b** Schematics of a linear polarizer consisting of three Au mirrors and a grating with the grooves in the vertical direction

was monitored by a photoelectron spectrometer and the single order selection was always confirmed. The photon flux of the 17th harmonic with circularly polarization was ~106 photons/pulse, comparable to that of linearly polarized light. The selected harmonic was detected by an electron multiplier (R2362, Hamamatsu Photonics) after the linear polarized described in the next section. The transmitted intensity $I(\phi)$ as a function of rotation angle of the polarizer ϕ was measured with an accumulation time of 3 s. every 10° between 0 and 180° for circular polarization and every 5° for linear polarization with an assumption that $I(\phi) = I(\phi - 180)$.

7.2.3 Characterization of Polarization

To characterize the polarization state of HHs, a linear polarizer for EUV light was constructed by three Au mirrors schematically shown in Fig. 7.4 [53], which has been used in EUV spectroscopy [54]. Intuitively, s-polarized light goes through the polarizer more because of the anisotropy in the reflectance of the Au mirror between s and p polarizations as listed in Table 7.1. These were calculated using the values in [55] and the Au mirrors with no coating were used to ensure the optical response of Au. In the constructed polarizer, the incident angles to the first and the third mirror were set as 70°, and that to the second mirror was set as 50° [53].

The Stokes vector of the completely polarized light beam $\overrightarrow{S} = (S_0, S_1, S_2, S_3)$ is associated with $I(\phi)$ as follows: when the phase difference between the x and y components of a polarized electric field of light is δ, of which sign determines the handedness of a circular polarization,

$$I(\phi) = \frac{I(0°) + I(90°)}{2} + \frac{I(90°) - I(0°)}{2}\cos(2\phi) + \sqrt{I(0°)}\sqrt{I(90°)}\sin(2\phi)\cos\delta. \tag{7.1}$$

The Stokes vector is associated with $I(\phi)$ by

$$\left(I(0°) + I(90°),\ \ I(90°) - I(0°),\ \ 2\sqrt{I(0°)}\sqrt{I(90°)}\cos\delta,\ \ 2\sqrt{I(0°)}\sqrt{I(90°)}\sin\delta\right) \tag{7.2}$$

Table 7.1 Reflectance and reflectance phase of Au [55]

Wavelength (nm)	Angle of incidence (°)	Reflectance		Phase (°)	
		$r_s{}^2$	$r_p{}^2$	δ_s	δ_p
50	70	0.515	0.251	−146	177
	50	0.251	0.0550	−16	151
47	70	0.455	0.199	− 46	179
	50	0.204	0.0332	−18	151

Hence, experimentally, S_2 is directly obtained by $I(45°) - I(-45°)$ and then, the absolute value of S_3 can also be evaluated. The sign of δ is usually determined by inserting a quarter waveplate. The ellipticity ε is given by $\varepsilon = \left|\tan\left(\frac{1}{2}\arctan\left(\frac{S_3}{\sqrt{S_1^2+S_2^2}}\right)\right)\right|$. Among the elements of the Stokes vector, there is a relationship of $S_0^2 = S_1^2 + S_2^2 + S_3^2$. However, when the beam contains the unpolarized component, these relationships are not directly applicable, because of $S_0^2 > S_1^2 + S_2^2 + S_3^2$, where S_0 corresponds to the total beam flux.

To take account of the unpolarized components and the diffraction by the gratings quantitatively, the transmittance of the optical system is evaluated by operating the Mueller matrixes, characterizing the optical components, on the Stokes vector [56]. The first element of the Stokes vector S_0 is proportional to $I(\phi)$, from which the Stokes vector and the optical parameters of the toroidal gratings are evaluated in this work. Using the complex reflection coefficients of an optical component $r_s \exp(i\delta_s)$ and $r_p \exp(i\delta_p)$ for s and p polarization, respectively, the Mueller matrix $\mathbf{M}$ for reflection is expressed as

$$\mathbf{M} = {}^1\!/_2\left(r_s^2 + r_p^2\right)\begin{pmatrix} 1 & -\cos 2\psi & 0 & 0 \\ -\cos 2\psi & 1 & 0 & 0 \\ 0 & 0 & \sin 2\psi \cos\Delta & \sin 2\psi \sin\Delta \\ 0 & 0 & -\sin 2\psi \sin\Delta & \sin 2\psi \cos\Delta \end{pmatrix}, \tag{7.3}$$

where $\tan\psi = r_p/r_s$ and $\Delta = \delta_p - \delta_s$ [53]. Because ψ and Δ depend on an incident angle θ, $\mathbf{M}$ at θ for Au is denoted as $\mathbf{M}_\theta$. In this work, to describe the diffraction by the grating, the matrix $\mathbf{M}_\mathrm{G}$ with the same formula as (7.3), using ψ_G and Δ_G defined by $\tan\psi_G = r_{TM}/r_{TE}$ and $\Delta_G = \delta_{TM} - \delta_{TE}$, respectively, is employed. Here, the complex coefficients for the transverse electric (TE) and transverse magnetic (TM) diffracted light are expressed as $r_{TE}\exp(i\delta_{TE})$ and $r_{TM}\exp(i\delta_{TM})$, respectively. Because the second toroidal grating in the TDCM is installed mirror-symmetrically including the groove geometry so that the light propagates in the backward direction of the diffraction [48], the Mueller matrix of the TDCM is expressed as $\mathbf{M}_\mathrm{G}\,\mathbf{M}_\mathrm{G}$ by the reciprocal theorem [57]. The rotation of the polarizer around the propagation direction of the light by ϕ is expressed as

$$\mathbf{R}(\phi) = \begin{pmatrix} 1 & 0 & 0 & 0 \\ 0 & \cos 2\phi & \sin 2\phi & 0 \\ 0 & -\sin 2\phi & \cos 2\phi & 0 \\ 0 & 0 & 0 & 1 \end{pmatrix}. \tag{7.4}$$

The Mueller matrix of the reflective polarizer rotated by ϕ is $\mathbf{R}(-\phi)\mathbf{M}_{70}\mathbf{M}_{50}\mathbf{M}_{70}\mathbf{R}(\phi)$. Here, $\mathbf{M}_{50}$ and $\mathbf{M}_{70}$ are calculated from the optical constants listed in Table 7.1. Consequently, $\overrightarrow{S}$ of the incident beam to the TDCM and the polarizer is transformed into $\overrightarrow{S'} = \mathbf{R}(-\phi)\mathbf{M}_{70}\mathbf{M}_{50}\mathbf{M}_{70}\mathbf{R}(\phi)\mathbf{M}_G\mathbf{M}_G\overrightarrow{S}$.

7.2.4 Polarization After the Time-Delay Compensated Monochoromator

Firstly, to examine whether the reflection polarizer works correctly, $I(\phi)$ of linearly polarized 17th harmonic (47 nm) with TE and TM polarizations were measured, as shown in Fig. 7.5a. Here, the direction of 0° is parallel to the groove of the toroidal grating and TE polarization. The TM polarization is perpendicular to the TE polarization. Transmitted intensity approaches to maximum in the same direction of the electric field, while the intensity of the perpendicular direction to the electric field was 0.033 of the maximum as expected from the extinction ratio of the polarizer calculated using the optical constants tabulated in Table 7.1. Hence, quantitatively, the three sets of Au mirrors work as a linear polarizer.

For the linear TE and TM polarizations of $\vec{S}_{\substack{TE\\TM}} = (1, \mp 1, 0, 0)$, the first element of $\vec{S}'_{\substack{TE\\TM}}$ after the TDCM and the polarizer is proportional to $\alpha \pm \beta\cos(2\phi)$ accordingly, where $\alpha = 1.69$ and $\beta = 1.58$ for the 17th harmonic obtained using ψ and Δ of Au. The difference between α and β is due to the finite reflectivity of the Au mirror of the orthogonal component in the polarizer. The solid lines in Fig. 7.5a indicate the fitting results for these equations. Although only the proportional coefficient was a fitting parameter, the angle dependence was reproduced. Therefore, the reflectance and the phase in Table 7.1 appropriately describes the responses of the Au mirrors installed in the reflection polarizer.

When the polarizations of the HHs were switched to circular polarizations, the angle dependences of the 17th harmonic selected by the TDCM were changed to those of Fig. 7.5c. The angle dependence shows that the polarizations after the TDCM are no longer circular polarization. In contrast with linear polarization, however, the LH CP light (●) has a maximum transmittance in the 325° direction, while the RH CP light (▲) has a maximum transmittance in the 35° direction. The angle dependence of the 16th harmonic was similar to that of the 17th harmonic as shown in Fig. 7.5b.

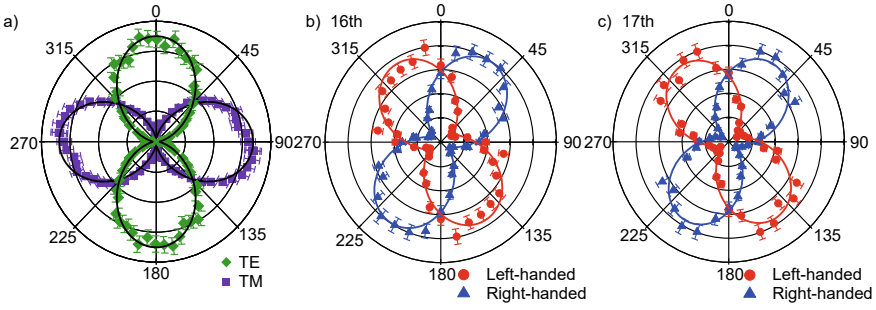

Fig. 7.5 **a** Transmitted intensities of TE (◆) and TM (■) polarizations of the 17th harmonic as a function of the rotating angle of the polarizer ϕ, respectively. The solid lines denote the fitting results. **b**, **c** Transmitted intensities of the left- (●) and right-handed (▲) CP 16th and 17th harmonics as a function of ϕ, respectively. The solid lines are the fitting results

Here, note that the circular polarization of the 16th and 17th harmonics are orthogonal to each other under the same generation condition. The difference in the tilt direction from 0° of the angular distribution between the 16th and17th harmonics confirms that they have the opposite circular polarization experimentally. The sensitive response of the angle dependence to circular polarization also suggests that the observed HHs are highly polarized. If the harmonics are non-polarized, the transmittance should have the minimum at 90° and 270°, while the experimentally observed minimum was observed in directions of ±55° and ±235°.

To understand the angle dependence of the transmittance of the RH and LH CP light including the unpolarized component with $\overrightarrow{S}_{\substack{RH\\LH}} = A(1,\ 0,\ 0,\ \pm 1) + B(1,\ 0,\ 0,\ 0)$, respectively, the first element of the Stokes vector $\overrightarrow{S}'_{\substack{RH\\LH}} = \mathbf{R}(-\phi)\mathbf{M}_{70}\mathbf{M}_{50}\mathbf{M}_{70}\mathbf{R}(\phi)\mathbf{M}_G\mathbf{M}_G \overrightarrow{S}_{\substack{RH\\LH}}$ is calculated. Here, A and B are proportional to the intensities of the polarized and nonpolarized components, respectively. The transmitted intensities of the RH and LH CP harmonics $I_{\substack{RH\\LH}}(\phi)$, i.e. the first element of $\overrightarrow{S}'_{\substack{RH\\LH}}$, are given as

$$I_{\substack{RH\\LH}}(\phi) = P + Q\cos(2\phi) \pm R\sin(2\phi) \tag{7.5}$$

where

$$P = (A + B)\alpha(1 + \cos^2(2\psi_G)), \tag{7.6}$$

$$Q = 2(A + B)\beta\cos(2\psi_G), \tag{7.7}$$

and

$$R = -A\beta\sin(2\Delta_G)\sin^2(2\psi_G). \tag{7.8}$$

For the 16th harmonic, $\alpha = 1.56$ and $\beta = 1.41$. Because R depends on Δ_G, the tilt direction of the principle axis of the transmittance depends on the circular polarization.

To evaluate the optical constants ψ_G and Δ_G, P, Q, and R are determined by fitting (7.5) to the experimental results. The fitting results are shown by the solid lines in Fig. 7.5b and c. ψ_G is uniquely determined by (7.6) and (7.7), while the other parameters, A, B, and Δ_G, cannot be determined uniquely. However, (7.7) and (7.8) limit the range of A as follows: (7.7) gives the maximum of A as $Q/(2\beta\cos(2\psi_G))$, where a HH is completely polarized, i.e. $B = 0$. Equation (7.8) also gives the lower limit of A as $R/\left(\beta\sin^2(2\psi_G)\right)$ to satisfy $R/\left(A\beta\sin^2(2\psi_G)\right) \leq 1$. Consequently, the range of A is given by

$$|R|/\left(\beta\sin^2(2\psi_G)\right) \leq A \leq Q/(2\beta\cos(2\psi_G)). \tag{7.9}$$

The corresponding range of B is given by (7.6) or (7.7) and, consequently, $\overrightarrow{S}_{\substack{RH\\LH}}$ and $\overrightarrow{S}'_{\substack{RH\\LH}}$ are also determined. Using these values, the corresponding Δ_G, degree of polarization (DOP) before and after the TDCM, and ellipticity ε after the TDCM are given. Here, DOP is defined by DOP $= \sqrt{S_1^2 + S_2^2 + S_3^2}/S_0$ for the Stokes vector of (S_0, S_1, S_2, S_3). In Table 7.2, ψ_G and the ranges of Δ_G, DOP, and ε are listed. Fortunately, the ranges of Δ_G, DOP, and ε are limited. Hence, we can discuss the polarization states further.

The CP HHs were reported to be partially depolarized, because of the dynamical symmetry breaking by medium ionization and the temporal evolution of the driving laser during the HH generation [58]. The DOP of the 17th harmonic was reported to be approximately 0.6 [58]. CP HHs generated in noncollinear scheme have a DOP of about 0.85 [44]. The depolarized components would be attributable to the ionization of the interacting gas, introducing decoherence in the process of HH generation. The DOP on target in the present work is 0.81 in the worst case, which is higher than that in [58]. On the gratings, only the spatially coherent component with the same polarization can be diffracted. Therefore, the gratings work as filters passing through the polarized component. Higher DOP is one advantage of this scheme.

The obtained ψ_G is close to those of Pt, $\psi = 36.6°$ for the 16th and $\psi = 36.0°$for the 17th harmonic, respectively, at the incident angle of 71° [55]. The phase shift of Pt, $\Delta = 319°$ for 16th and $\Delta = 321°$ for 17 harmonics, are also within the range of Δ_G. Although the harmonics are not reflected but diffracted on the surface of the toroidal grating, the diffraction efficiency depends on the coated substance, Pt. Therefore, it is reasonable that ψ_G and Δ_G have similar values to those of Pt. The ratio of the diffraction efficiency ${r_{TM}}^2/{r_{TE}}^2$ of the toroidal grating is related with ψ_G by $\tan\psi_G = r_{TM}/r_{TE}$, and it is 0.66 when the average value of $\psi_G = 39.0°$ is employed for the 17th harmonic. This value is consistent with the experimentally measured value 0.70 ± 0.05 at 47 nm for linearly polarized light. The experimentally determined range of ε shows that the circular polarization of the selected single-order harmonics was deteriorated by the TDCM, owing to the anisotropy and the phase shift by diffraction.

Table 7.2 Parameters for right (RH)- and left-handed (LH) circularly polarized harmonics after TDCM

Harmonic order	Polarization	ψ_G (°)	Δ_G (°)	DOP before TDCM	DOP after TDCM	Ellipticity
16	LH	39.6	315~338	0.71~1.00	0.81~1.00	0~0.38
	RH	39.8	315~329	0.88~1.00	0.91~1.00	0~0.24
17	LH	39.7	315~330	0.87~1.00	0.90~1.00	0~0.24
	RH	38.2	315~329	0.88~1.00	0.91~1.00	0~0.23

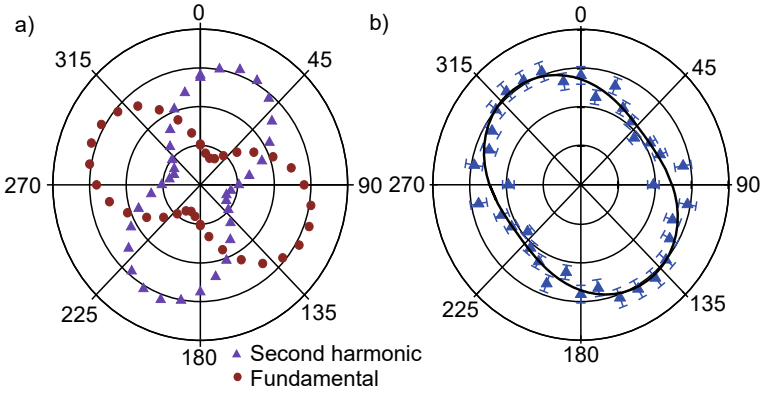

Fig. 7.6 **a** Transmitted intensities of elliptically polarized fundamental light ω (●) and the second harmonic 2ω (▲) as a function of the rotating angle of the polarizer. **b** Transmitted intensities of RH elliptically polarized 17th harmonic as a function of the rotating angle of the linear polarizer. The solid lines are the fitting results of (7.10) and (7.11). These two results are overlapped

7.2.5 Compensation of Ellipticity for Circluar Polarization

One approach to obtain the CP harmonic at focus in this scheme is to generate elliptically polarized HHs and to correct the ellipticity by the anisotropic diffraction and the phase shift of the toroidal gratings. For example, the elliptical polarization along the TM direction is preferred, because the diffraction efficiency of TE mode is higher than that of TM mode. To generate elliptically polarized HHs, the polarization of ω with higher pulse energy than 2ω was set to parallel to TM mode and the ellipticity was introduced to the driving laser field by rotating the AQW from the optimum angle for the quarter wavelength. When the angle was rotated by 20° from the optimum angle, the polarizations of the driving laser field were changed to be elliptical. Figure 7.6a shows the angle dependence of the RH ω and LH 2ω intensities measured using a linear polarizer. The ellipticities of ω and 2ω were 0.48 and 0.52, respectively.

These two laser fields were synthesized and generated the RH 17th harmonic, of which angle dependence of the intensity is shown in Fig. 7.6b. Because the optical parameters of the toroidal grating listed in Table 7.2 are not uniquely determined, $I(\phi)$ of $\overrightarrow{S} = (S_0, S_1, S_2, S_3)$ are evaluated for two extreme cases with $\Delta_G = 329°$ and with $\Delta_G = 315°$. The corresponding $I(\phi)$ are

$$I(\phi) = 1.747S_0 - 0.625S_1 + (0.584S_0 - 1.633S_1)\cos(2\phi) + (-0.750S_2 + 1.328S_3)\sin(2\phi) \tag{7.10}$$

and

$$I(\phi) = 1.747S_0 - 0.625S_1 + (0.584S_0 - 1.633S_1)\cos(2\phi) + 1.525S_3\sin(2\phi). \tag{7.11}$$

The fitting these equations to the experimental data determines S_0 and S_1 uniquely. However, S_2 and S_3 have ambiguities, although the coefficient for $\sin(2\phi)$ can be determined. Table 7.2 suggests that the selected harmonic by the TDCM has higher DOP than ca. 0.9. Therefore, DOP is here assumed to be 0.90 and $\overrightarrow{S}$ was determined, although DOP might be changed when the HH is generated by the laser field synthesized by elliptically polarized lights. The fitting results to (7.10) and (7.11) are shown by the solid lines in Fig. 7.6b. Two fitting results are almost overlapped. $\overrightarrow{S} = (1.00, 0.31, 0.73, 0.43)$ for $\Delta_G = 329°$ and $\overrightarrow{S} = (1.00, 0.31, 0.83, 0.17)$ for $\Delta_G = 315°$ are obtained. The corresponding Stokes vectors after the TDCM are $\mathbf{M}_G\mathbf{M}_G\overrightarrow{S} = (1.00, -0.05, -0.02, 0.89)$ with $\varepsilon = 0.94$ and $\mathbf{M}_G\mathbf{M}_G\overrightarrow{S} = (1.00, -005, -0.18, 0.87)$ with $\varepsilon = 0.80$. The latter case gives the lowest ellipticity under the conditions given in Table 7.2. Therefore, it is confirmed that the diffracted single-order 17th harmonic has an ellipticity better than 0.80. This ellipticity is applicable to the measurement of the photoelectron angular distribution [58] and of magnetic imaging [46]. The compensation of the ellipticity is shown by the shift of $\overrightarrow{S}$ denoted by the sphere (●) before the TDCM to the square (■) after the TDCM on the Poincare sphere in Fig. 7.7.

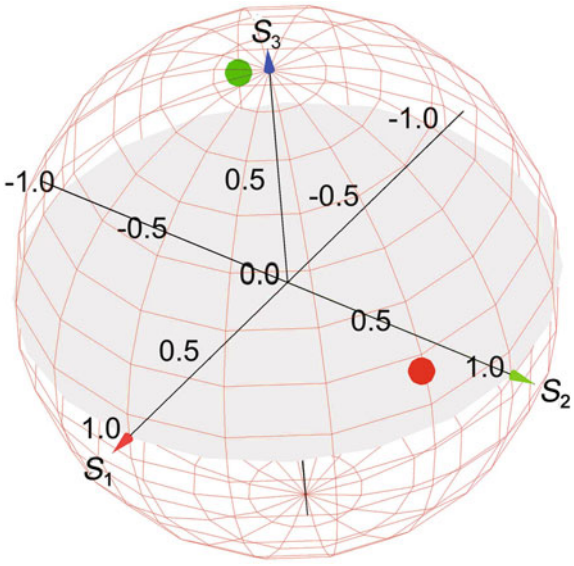

Fig. 7.7 Polarization states on the Poincare sphere. The sphere (●) and square (■) show the Stokes vectors of the 17th harmonic, generated elliptically polarized laser field, before and after the TDCM, respectively

7.3 Summary

In this work, the polarizations of the monochromatized 16th and 17th harmonics of a Ti:sapphire laser by the TDCM were characterized for the development of ultrashort CP EUV light source. It was found that the circular polarization was distorted by the diffraction on the toroidal gratings. However, the diffraction on the grating increases DOP. The compensation of the ellipticity by manipulating the driving laser field was demonstrated for the first time. Here, we assumed DOP = 0.9 in reference to the case driven by CP driving lasers. The single-order CP HH pulses selected by the TDCM will be a versatile light source for the investigation of magnetism and chirality.

In this article, we presented two topics related with molecular chirality. The first topic is the chiral responses of limonene molecules in HHG. We are interested in the nonlinear responses of other chiral molecules. The chirality in the electronic states of a chiral molecules should be related with HHG. We will investigate other chiral molecules. In the second topic, we are interested in the application of the CP HH light source to photoelectron spectroscopy of chiral molecules.

Acknowledgements MEXT Q-LEAP (JPMXS0118068681); JST CREST (JPMJCR15N1); KAKENHI (19H01814).

References

1. R. Cireasa, A.E. Boguslavskiy, B. Pons, M.C.H. Wong, D. Descamps, S. Petit, H. Ruf, N. Thiré, A. Ferré, J. Suarez et al., Nat. Phys. **11**, 654 (2015)
2. D. Baykusheva, H.J. Wörner, Phys. Rev. X **8**, 031060 (2018)
3. D. Baykusheva, D. Zindel, V. Svoboda, E. Bommeli, M. Ochsner, A. Tehlar, H.J. Wörner, Proc. Natl. Acad. Sci. USA **116**, 23923 (2019)
4. F. Krausz, M. Ivanov, Rev. Mod. Phys. **81**, 163 (2009)
5. P.B. Corkum, Phys. Rev. Lett. **71**, 1994 (1993)
6. B. Vodungbo, A.B. Sardinha, J. Gautier, G. Lambert, C. Valentin, M. Lozano, G. Iaquaniello, F. Delmotte, S. Sebban, J. Lüning et al., Opt. Express **19**, 4346 (2011)
7. A. McPherson, G. Gibson, H. Iara, H. Johann, T.S. Luk, I.A. McIntyre, K. Boyer, C.K. Rodes, J. Opt. Soc. Am. B **4**, 595 (1987)
8. M. Ferray, A. L'Huillier, X.F. Li, L.A. Lompre, G. Mainfray, C. Manus, J. Phys. B: At. Mol. Opt. Phys. **21**, L31 (1988)
9. M. Hentschel, R. Kienberger, C. Spielmann, G.A. Reider, N. Milosevic, T. Brabec, P. Corkum, U. Heinzmann, M. Drescher, F. Krausz, Nature **414**, 509 (2001)
10. T. Sekikawa, A. Kosuge, T. Kanai, S. Watanabe, Nature **432**, 605 (2004)
11. Y. Nabekawa, T. Shimizu, T. Okino, K. Furusawa, H. Hasegawa, K. Yamanouchi, K. Midorikawa, Phys. Rev. Lett. **97**, 153904 (2006)
12. K. Zhao, Q. Zhang, M. Chini, Y. Wu, X. Wang, Z. Chang, Opt. Lett. **37**, 3891 (2012)
13. T. Gaumnitz, A. Jain, Y. Pertot, M. Huppert, I. Jordan, F. Ardana-Lamas, H.J. Wörner, Opt. Express **25**, 27506 (2017)
14. Y. Harada, E. Haraguchi, K. Kaneshima, T. Sekikawa, Phys. Rev. A **98**, 021401(R) (2018)
15. K. Ito, E. Haraguchi, K. Kaneshima, T. Sekikawa, Opt. Express **27**, 38735 (2019)
16. P. Fischer, F. Hache, Chirality **17**, 421 (2005)

17. B. Ritchie, Phys. Rev. A **13**, 1411 (1976)
18. N. Böwering, T. Lischke, B. Schmidtke, N. Müller, T. Khalil, U. Heinzmann, Phys. Rev. Lett. **86**, 1187 (2001)
19. T. Lischke, N. Böwering, B. Schmidtke, N. Müller, T. Khalil, and U. Heinzmann, Phys. Rev. A **70**, 022507 (2004).
20. M.H.M. Janssen, I. Powis, Phys. Chem. Chem. Phys. **16**, 856 (2014)
21. D.B. Milošević, W. Becker, R. Kopold, Phys. Rev. A **61**, 063403 (2000)
22. A. Fleischer, P. Sidorenko, O. Cohen, Opt. Lett. **38**, 223 (2013)
23. A. Fleischer, O. Kfir, T. Diskin, P. Sidorenko, O. Cohen, Nat. Photon. **8**, 543 (2014)
24. L. Medišauskas, J. Wragg, H.v.d. Hart, M.Y. Ivanov, Phys. Rev. Lett. **115**, 153001 (2015)
25. O. Kfir, P. Grychtol, E. Turgut, R. Knut, D. Zusin, D. Popmintchev, T. Popmintchev, H. Nembach, J.M. Shaw, A. Fleischer et al., Nat. Photon. **9**, 99 (2015)
26. T. Fan, P. Grychtol, R. Knut, C. Hernández-García, D.D. Hickstein, D. Zusin, C. Gentry, F.J. Dollar, C.A. Mancuso, C.W. Hogle et al., Proc. Natl. Acad. Sci. USA **112**, 14206 (2015)
27. D. Baykusheva, M.S. Ahsan, N. Lin, H.J. Wörner, Phys. Rev. Lett. **116**, 123001 (2016)
28. D. Wang, X. Zhu, L. L. Xi Liu, X. Zhang, P. Lan, P. Lu, Opt. Express **25**, 23502 (2017).
29. D. Baykusheva, S. Brennecke, M. Lein, H.J. Wörner, Phys. Rev. Lett. **119**, 203201 (2017)
30. Á. Jiménez-Galán, N. Zhavoronkov, M. Schloz, F. Morales, M. Ivanov, Opt. Express **25**, 22880 (2017)
31. E.O. Hulburt, Astrophys. J. **54**, 116 (1921)
32. M. Lewenstein, P. Balcou, M.Y. Ivanov, A. L'Huillier, P.B. Corkum, Phys. Rev. A **49**, 2117 (1994)
33. O. Smirnova, Y. Mairesse, S. Patchkovskii, J. Phys. B: At. Mol. Opt. Phys. **48**, 234005 (2015)
34. O. Kfir, E. Bordo, G.I. Haham, O. Lahav, A. Fleischer, O. Cohen, Appl. Phys. Lett. **108**, 211106 (2016)
35. O. Kfir, P. Grychtol, E. Turgut, R. Knut, D. Zusin, A. Fleischer, E. Bordo, T. Fan, D. Popmintchev, T. Popmintchev, J. Phys. B: At. Mol. Opt. Phys. **49**, 123501 (2016)
36. E.S. Toma, P. Antoine, A.d. Bohan, H.G. Muller, J. Phys. B: At. Mol. Opt. Phys. **32**, 5843 (1999)
37. P. Brint, E. Meshulam, A. Gedanken, Chem. Phys. Lett. **109**, 383 (1984)
38. M.M.R. Fanood, M.H.M. Janssen, I. Powis, J. Chem. Phys. **145**, 124320 (2016)
39. M. Carnell, S.D. Peyerimhoff, A. Breest, K.H. Gödderz, P. Ochmann, J. Hormes, Chem. Phys. Lett. **180**, 477 (1991)
40. F. Pulm, J. Schramm, J. Hormes, S. Grimme, S.D. Peyerimhoff, Chem. Phys. **224**, 143 (1997)
41. M.F. Rodrigues, M.G. Bernardo-Gil, J. Chem. Eng. Data **40**, 1193 (1995)
42. T. Adachi, K. Kondo, S. Watanabe, Appl. Phys. B **55**, 323 (1992)
43. D.D. Hickstein, F.J. Dollar, P. Grychtol, J.L. Ellis, R. Knut, C. Hernández-García, D. Zusin, C. Gentry, J.M. Shaw, T. Fan et al., Nat. Photon. **9**, 743 (2015)
44. P.-C. Huang, C. Hernández-García, J.-T. Huang, P.-Y. Huang, C.-H. Lu, L. Rego, D.D. Hickstein, J.L. Ellis, A. Jaron-Becker, A. Becker et al., Nat. Photon. **12**, 349 (2018)
45. D. Azoury, O. Kneller, M. Krüger, B.D. Bruner, O. Cohen, Y. Mairesse, N. Dudovich, Nat. Photon. **13**, 198 (2019)
46. O. Kfir, S. Zayko, C. Nolte, M. Sivis, M. Möller, B. Hebler, S.S.P.K. Arekapudi, D. Steil, S. Schäfer, M. Albrecht et al., Sci. Adv. **3**, eaao4641 (2017)
47. L. Poletto, P. Villoresi, E. Benedetti, F. Ferrari, S. Stagira, G. Sansone, M. Nisoli, Opt. Lett. **32**, 2897 (2007)
48. M. Ito, Y. Kataoka, T. Okamoto, M. Yamashita, T. Sekikawa, Opt. Express **18**, 6071 (2010)
49. H. Igarashi, A. Makida, M. Ito, T. Sekikawa, Opt. Express **20**, 3725 (2012)
50. A. Makida, H. Igarashi, T. Fujiwara, T. Sekikawa, Y. Harabuchi, T. Taketsugu, J. Phys. Chem. Lett. **5**, 1760 (2014)
51. R. Iikubo, T. Fujiwara, T. Sekikawa, Y. Harabuchi, S. Satoh, T. Taketsugu, Y. Kayanuma, J. Phys. Chem. Lett. **6**, 2463 (2015)
52. R. Iikubo, T. Sekikawa, Y. Harabuchi, T. Taketsugu, Faraday Discuss. **194**, 147 (2016)

53. T. Koide, T. Shidara, M. Yuri, N. Kandaka, K. Yamaguchi, H. Fukutani, Nucl. Instrum. Methods Phys. Res. **308**, 635 (1991)
54. W.R. Hunter, in *Vacuum Ultraviolet Spectroscopy I*, ed. by J.A. Samson, D.L. Ederer (Academic Press, San Diego, 1998)
55. W.S.M. Werner, K. Glantschnig, C. Ambrosch-Draxl, J. Phys. Chem. Ref. Data **38**, 1013 (2009)
56. R.M.A. Azzam, J. Opt. Soc. Am. A **33**, 1396 (2016)
57. D. Maystre, *Edited by E* (Université d'Aix-Marseille, CNRS, Popov (Institut Fresnel, 2014).
58. L. Barreau, K. Veyrinas, V. Gruson, S.J. Weber, T. Auguste, J.-F. Hergott, F. Lepetit, B. Carré, J.-C. Houver, D. Dowek et al., Nat. Commun. **9**, 4727 (2018)